Adaptive Equalization System for Visible Light Wireless Communication Utilizing Multiple White LED Lighting Equipment

Toshihiko Komine, *Member, IEEE,* Jun Hwan Lee, Shinichiro Haruyama, *Member, IEEE,* and Masao Nakagawa, *Fellow, IEEE*

***Abstract*—White LEDs were invented the 1990's. Since then they have been extensively researched and applied in various ways. Compared with conventional lighting devices, the white LED has lower power consumption, lower voltage requirements, longer lifetime, smaller size, faster response, and cooler operation. The white LED will eventually replace incandescent or fluorescent lights in offices and homes.**

We have proposed an indoor visible light wireless communication system that utilizes multiple white LED lighting equipment. In this system, the equipment is used not only for illuminating rooms but also for an optical wireless communication system. The system has significantly higher power levels than infrared wireless communication systems, since it also functions as the main lighting equipment. One problem is we tend to install many lighting sources on a ceiling in order to illuminate the room as evenly as possible. While the number of sources permits site diversity transmission over LOS links, the optical path difference between the multiple sources triggers intersymbol interference (ISI), which significantly degrades system performance.

This paper overcomes the ISI problem by proposing an adaptive equalization system. We elucidate the most effective training sequence interval for channel estimation in a mobile environment. And we show that the adaptive equalization system with the effectual interval alleviates the influence of shadowing.

***Index Terms*—Optical communication, light-emitting diodes, lighting, communication systems, adaptive equalizers, wireless LAN.**

I. Introduction

In the 21st century, high data rate transmission will play a pervasive role in our life. To achieve high data rate transmission, radio frequencies are the dominant choice in offices and homes. However, the radio frequency spectrum is so congested that it will be impossible to provide a truly ubiquitous high data rate service. We need a new wireless medium.

One exciting new wireless medium has emerged with the development of the InGaN light emitting diode (LED). With the recent release of blue and green LEDs, we can create highly efficient white light sources by combining the three primary colors (red, green, and blue). The white LED is a strong candidate for the future lighting technology [1], [2]. Compared with conventional lighting methods, the white LED has lower power consumption, lower voltage requirements, longer lifetime, smaller size, and cooler operation. The Ministry of Economy, Trade and Industry of Japan estimates that if half of all incandescent and fluorescent lamps currently in use were replaced by LEDs, Japan could save the equivalent output of six mid-size power plants, and reduce the production of greenhouse gases. A national program underway in Japan has already suggested that white LED deserves to be considered as a general lighting technology of the 21st century to offset the growth in electric power energy consumption.

A group including the author has proposed an optical wireless communication system that employs white LEDs for indoor wireless networks [3]–[12]. In this system, LEDs are used not only as lighting devices, but also as communication devices. The system employs visible light, free-space optical wireless communication links. This dual function, lighting and communication, creates many new and interesting applications. The communication function is released by modulating the sources at rates that preclude visible flicker. The system has much higher power levels than an infrared system and a large radiation pattern at the sources (transmitters) since they also function as lighting devices. This means that the system has a specific impulse response that is different from that of infrared communication. The specific delay profile and the basic communication performance were evaluated in [6]. It was shown in [6] that the BER performance of the indoor visible light wireless system is degraded significantly by the effects of intersymbol interference (ISI). Here, we define the ISI as interference by path delay of same signal.

The zero forcing decision feedback equalizer (ZF-DFE) is generally applied to mitigate the effects of ISI in infrared wireless systems [13], [14]. However the performance of visible light wireless systems that use equalizers has not been clarified. Prior works on infrared wireless systems with equalizers assume that the impulse response is known to the receiver [15]. They also assume that the impulse response is static during each communication session. These assumptions are appropriate in infrared wireless communications because tracking is required by the low transmission power needed for eye-safety. And the receiver has to be the small FOV for achieving the high signal-to-noise ratio (SNR). Therefore, since the optical path is blocked easily by a pedestrian, connection is closed often. However, visible light wireless

Manuscript received May 14, 2006; revised October 17, 2006 and March 15, 2007; accepted March 30, 2007. The associate editor coordinating the review of this paper and approving it for publication was J. Tugnait.

The authors are with the Department of Information and Computer Science, Faculty of Science and Technology, Keio University, Kanagawa, 223–8522, Japan (e-mail: {komine, jhlee, haruyama, nakagawa}@nkgw.ics.keio.ac.jp).

Digital Object Identifier 10.1109/TWC.2009.060258

communication system can achieve sufficient SNR based on the large transmission power by the lighting function, even if the field-of-view (FOV) of receiver is large and the system has no tracking structure [6]. And the receiver can be mobile and have seamless communication. Therefore, the system can have dynamic impulse response by the move of terminal or pedestrian.

In this paper, we propose an adaptive equalization system and evaluate its performance in a visible light wireless system. Moreover, we discuss the influence of shadowing. We transmit training sequences and estimate the channel by the least mean square (LMS) algorithm. Incidentally, the modulation bandwidths of recent white LEDs in typical low cost lighting sources range from 10 MHz to 100 MHz. Recently, Resonant Cavity LEDs (RCLED) have been developed. The modulation bandwidth of RCLEDs is achieved to approximately 500 MHz [16]–[18]. Moreover, by using a pre-emphasis circuit at transmitter, the extension of the modulation bandwidth[1] is reported [19]. As mentioned above, recently, a considerable number of studies have been conducted on extension of wide modulation bandwidth. Therefore, it is important to study the visible light wireless communication system with adaptive equalizer at high speed data transmission. In addition, the adaptive equalization system is a promising approach to the compensation of the frequency response of white LED devices. In other words, the adaptive equalization system enables the development of a high speed communication system. Computer simulations show the most effective training sequence interval for channel estimation. The simulation results show that a visible light wireless system with adaptive equalization is robust against shadowing and can accommodate more connections.

II. Lighting Design and Basic Performance

We will discuss the communication performance of a typical visible light wireless environment: a small office with general lighting requirements. The room is $5 \times 5 \times 3$ m^3. A 2×2 lighting grid with communication function is installed on the ceiling. The center positions each node are A: 1.0, 1.0, 3.0), B: 4.0, 1.0, 3.0, C: 1.0, 4.0, 3.0, and D: 4.0, 4.0, 3.0), respectively. Each lighting source has 10×10 LEDs. LED spacing is 4 cm. Each LED has a semiangle of half power of 80.0 deg., center luminous intensity of 23.81 cd, and optical output power of 0.452 W. These represent the measured and calculated values of the commercial product LXHL-LW6C. The ceiling, wall, and floor have reflective index values of 0.8, 0.5, and 0.2, respectively. We assume that the receiver lies on a desk. The height of the desk is 0.85 m.

A. Illuminance Distribution Based on Lighting Engineering

We now describe our algorithm for calculating multiple-bounce horizontal illuminance. Although true reflections contain both specular and diffusive components [20], [21], we make the assumption that all reflectors are purely diffusive, ideal Lambertian. Experiments have shown that many typical materials such as plaster walls, acoustic-tiled walls, carpets, and unvarnished wood are well-approximated as Lambertian reflectors [21]–[24]. The radiation intensity pattern emitted by a differential element of an ideal diffuse reflector is independent of the angle of the incident light [25]. It is further assumed that each LED has a Lambertian radiation pattern.

Light from the source can reach the receiver after any number of reflections. Therefore, the horizontal illuminance can be written as an infinite sum [26]:

$$E = \sum_{n=0}^{\infty} E_n, \tag{1}$$

where E_n is the horizontal illuminance of the light undergoing exactly n reflections. The LOS horizontal illuminance E_0 is given by [25], [26]

$$E_0 = \sum_i \frac{I(0)\cos^m \phi_i}{{d_i}^2} \cos \psi_i, \tag{2}$$

higher order terms ($n > 0$) can be calculated recursively [22]:

$$E_n = \int_{wall} \frac{E_{n-1}}{\pi d^2} \rho \cos\phi \cos\psi dA_{wall}. \tag{3}$$

The integrations in Eq. (3) are performed with respect to the position on the surface of all reflectors. Here, the index i is ith LED element, $I(0)$ is luminous intensity on the optical axis, d is the distance between transmitter and receiver, m is Lambertian factor, ϕ is irradiance angle, ψ is incidence angle, dA_{wall} is the differential area of the reflector surface at the position, and ρ is the reflectivity at the position. Intuitively, it says that the n-bounce horizontal illuminance from a single point-source can be found by first finding the distribution and timing of the power from the point-source onto the reflecting walls; then, using the walls as a distributed light source, and then computing the (n-1)-bounce horizontal illuminance.

We give here a consideration of the illuminance of lighting equipment. In general, the illuminance of lights is standardized by ISO (International Organization for Standardization). By this set of standards, an illuminance between 300 and 1500 lx is required for office work [26]. A general recommendation is that the illuminance on the desk be uniform. The uniformity illuminance ratio is defined as the ratio of the minimum to the average illuminance. The uniformity ratio should be over 0.7 according to lighting engineers.

Figure 1(a) shows the distribution of horizontal illuminance, based on a numerical analysis at the optical receiver on the desk. Here, we simulated 10-bounce horizontal illuminance. We set the differential area of the reflector surface at 12.5 $\times$ 12.5 cm^2. From the figure, sufficient illuminance, 300 to 1500 lx (according to ISO), is obtained at the all places in the room. Therefore, this result shows that the setting of the lighting equipment provides acceptable illuminance according to the standards and good practices.

B. Average Received Optical Power

The average received optical power can be written as an infinite sum:

$$P_r = \sum_{n=0}^{\infty} P_{rn}, \tag{4}$$

[1]650 nm RCLED, 73 MHz $\rightarrow$ 224 MHz

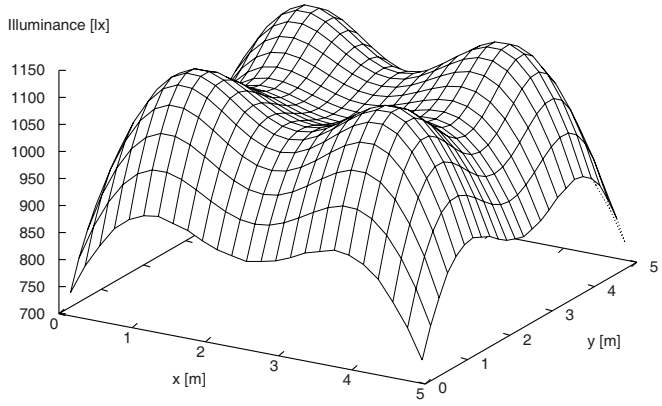

(a) Illuminance distribution. (Max.: 1124.2 lx, Min.: 737.2 lx, Ave.: 1008.1 lx, Uniformity ratio: 0.73)

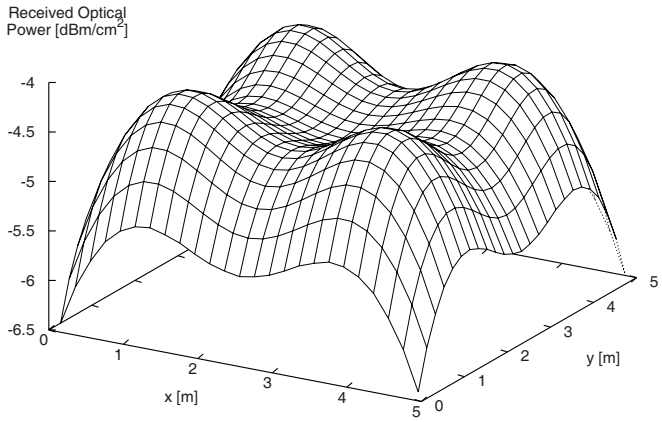

(b) Received optical power distribution. (Non Tracking, FOV 90 deg., Max.: -4.23 dBm/cm^2, Min.: -6.44 dBm/cm^2, Ave.: -4.81 dBm/cm^2)

Fig. 1. Illuminance distribution and received optical power distribution.

where n is the number of reflections. The LOS average received optical power P_{r0} is derived by the average transmitted optical power at each LED element P_{ti}, as follows,

$$P_{r0} = \sum_i P_{ti} H_i(0); \tag{5}$$

higher order terms ($n > 0$) can be calculated recursively:

$$P_{rn} = \int_{wall} \frac{P_{rn-1}}{\pi d^2} \rho \cos\phi \cos\psi dA_{wall}. \tag{6}$$

The integrations in Eq. (6) are performed with respect to the position on the surface of all reflectors. Here, the index i is ith LED element, d is the distance between transmitter and receiver, ϕ is irradiance angle, ψ is incidence angle, dA_{wall} is the differential area of the reflector surface at the position, and ρ is the reflectivity at the position. Here, the channel can be described in terms of the frequency response [27]

$$H(f) = \int_{-\infty}^{\infty} h(t) e^{-j2\pi ft} dt, \tag{7}$$

which is the Fourier transform of impulse response $h(t)$. The frequency response of optical channels are relatively flat near DC, so for most purposes, the single most important quantity characterizing a channel is the DC gain $H(0)$ [27]. The channel DC gain on directed path is given as:

$$H(0) = \begin{cases} \dfrac{(m+1)A}{2\pi d^2} \cos^m \phi T_s(\psi) g(\psi) cos\psi, & 0 \le \psi \le \Psi_c \\ 0, & \psi > \Psi_c, \end{cases} \tag{8}$$

where m is Lambertian factor, A is the physical area of the detector in a photodiode(PD), and Ψ_c is the concentrator FOV (semiangle). The parameters used in the received optical power calculation are set as follows. $T_s(\psi)$=1, $g(\psi)$=1, A=1 cm^2.

To alleviate the shadowing problem, we assume a diversity system that utilizes the multiple lighting sources. All sources transmit the same OOK modulated signals synchronously. A main HUB is positioned at the center of the ceiling and connected to each source. Figure 1(b) shows the received optical power at the receiver across the room. We can see that the received power is very high, compared to that achieved by an infrared wireless communication system[2] We can also see that the received optical power is small at the corners of the room. Considering actual situations, we seldom use a terminal in the corner of a room. Right under the lighting equipment, the received power is high.

C. Propagation Delay by Multiple Lighting Equipments

In the transmission system, the electrical transmission data is modulated by OOK. The modulated signal is transmitted by LEDs. In the LEDs, the electrical signal is converted to optical signal. Here we define $X(t)$ as the transmitted optical signal. Here $X(t)$ = 0 or 1.

At the receiver, delayed transmitted optical signals are received at one time, and the received optical signal is converted to electrical signal at PD. The O/E convergence efficiency at PD is R. Here, the delayed electrical signal is shown as convolution of optical wireless channel $h(t)$. The electrical signal is added the additive white Gaussian noise (AWGN).

The optical wireless channel model used here is expressed as follows:

$$Y(t) = RX(t) \otimes h(t) + N(t), \tag{9}$$

where symbol $\otimes$ denotes convolution. And here, we assume that LED and PD have linear converter. While Eq. (9) is simply a conventional linear filter channel with additive noise, visible light systems differ from conventional electrical or radio systems in several respects. Because the channel input $X(t)$ represents instantaneous optical power, the channel input is nonnegative $X(t) \ge 0$, and the average transmitted optical power P_t is given by $P_t = \lim_{T\to\infty} \frac{1}{2T} \int_{-T}^{T} X(t)dt$ rather than the usual time-average of $|X(t)|^2$, which is appropriate when X(t) represents amplitude.

In the visible light wireless system, the LEDs are distributed across the ceiling and have wide irradiance distribution for

[2]In [15], the received optical power in infrared wireless communication is calculated. The received optical power is 2.4 mW/cm^2 = -26.20 dBm/cm^2 (LOS link, w/o tracking). On the other hand, in our paper, the received optical power is -4.81 dBm/cm^2 (average). Therefore, visible light wireless communication system has gain about 20 dB, compared with generic infrared wireless communication system.

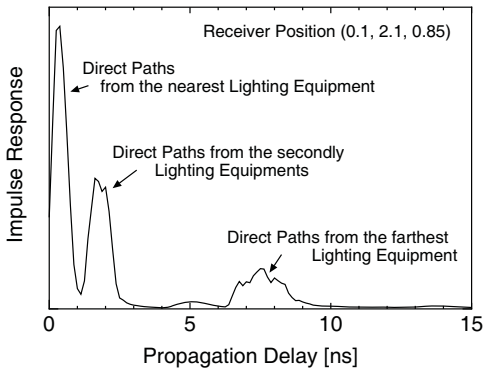

Fig. 2. Impulse response at (0.1, 2.1, 0.85).

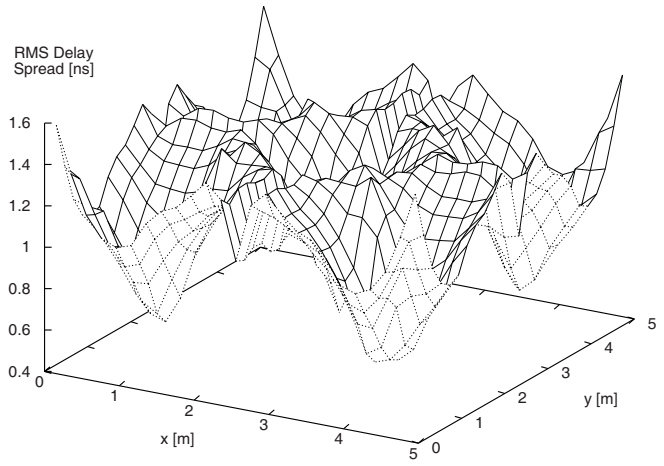

Fig. 3. RMS delay spread (FOV 90 deg., Max.: 1.58 ns, Min.: 0.55 ns, Ave.: 1.13 ns).

achieving adequate general lighting. Thus a non-directed line-of-sight (LOS) path is assumed. Since we calculate the impulse response by ray-tracing, the impulse response differs depending on the position of the receiver [27].

Here, we define the impulse response as the sum of received signals from the lighting sources and walls when an impulse is input to HUB in the ceiling. Figure reffig:imp shows the impulse response at (0.1, 2.1, 0.85). From the figure, we can see that the first peak consists mainly of the direct path from the nearest source. The next peak consists mainly of the direct paths from secondary sources. After some delay, the lights from the farthest source and reflected lights are received. In the visible light wireless system, the sources are spread across large areas. In infrared wireless communication, large surface areas, like 40 cm $\times$ 40 cm, are not commercially feasible. It is clear that the receiver of the visible light wireless system has an impulse response that differs from that of an infrared wireless system.

A useful measure of the severe ISI induced by a multipath channel, $h(t)$, is the channel root mean square (RMS) delay spread τ_{RMS}. The RMS delay spread of a channel is a remarkably accurate predictor of ISI induced SNR penalty, independent of the particular time dependence of that channel's impulse response [27]. The RMS delay spread is computed from the impulse response using

$$\tau_{RMS} = \sqrt{\frac{\int_{-\infty}^{\infty}(t-\tau_0)^2 h^2(t)dt}{\int_{-\infty}^{\infty} h^2(t)dt}}, \tag{10}$$

where the mean delay time τ_0 is given by

$$\tau_0 = \frac{\int_{-\infty}^{\infty} t \cdot h^2(t)dt}{\int_{-\infty}^{\infty} h^2(t)dt}. \tag{11}$$

The impulse response $h(t)$ and RMS delay spread τ_{RMS} can be considered to be deterministic quantities, in the sense that as long as the positions of the transmitter, receiver and intervening reflectors are fixed, $h(t)$ and τ_{RMS} are fixed. This stands in contrast to the case of time varying radio channels, where the RMS delay spread is interpreted as a statistical expectation of a random process [28].

Figure 3 shows the distribution of RMS delay spread at each position of the receiver. From this figure, the RMS delay spread is small at the position right under each source. We know the RMS delay spread consists mainly of the delay between sources. In radio wireless communication, the typical RMS delay spread is 25 to 50 ns in office buildings in urban areas [29]. In the visible light wireless system, on the other hand, it is below a few ns. One reason is that the much larger wavelength, compared to visible light, makes radio wave reflections appear to be specular reflections. Besides, radio waves can penetrate through walls from one room to another, leading to longer path lengths. Therefore, the visible light wireless system is much less sensitive to ISI than radio wireless systems.

D. Electrical SNR

We show some numerical and simulation results. Here, we assume the noise model is AWGN model. In an optical channel, originally, the quality of transmission is dominated by shot noise. The desired signals contain a time-varying shot noise process which has an average rate of 10^4 to 10^5 photons/bit. In our channel model, however intense ambient light striking the detector leads to a steady shot noise having a rate of order of 10^7 to 10^8 photons/bit, even if a receiver employs a narrow-band optical filter. Therefore, we can neglect the shot noise caused by signals and model the ambient-induced shot noise as a Gaussian process [30]. The electrical SNR is expressed as

$$SNR = \frac{(RP_r)^2}{\sigma_{shot}^2 + \sigma_{thermal}^2}, \tag{12}$$

where R is the detector responsivity. The shot noise variance is given by [31]

$$\sigma_{shot} = 2qRP_rB + 2qI_{bg}I_2B, \tag{13}$$

where q is the electronic charge, B is equivalent noise bandwidth, I_{bg} is background current. I_2, noise bandwidth factor, is set to 0.562. The thermal noise variance is given by

$$\sigma_{thermal} = \frac{8\pi kT_k}{G}\eta A I_2 B^2 + \frac{16\pi^2 kT_k\Gamma}{g_m}\eta^2 A^2 I_3 B^3, \tag{14}$$

The first term represents the thermal noise from the feedback resistor; k is Boltzmann's constant, T_k is absolute temperature,

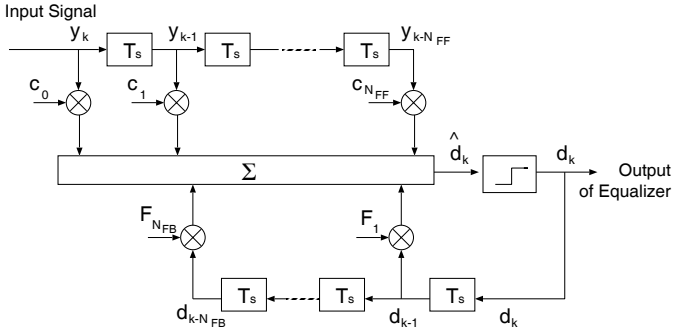

Fig. 4. Decision feedback equalizer.

and G is the open-loop voltage gain, η is the fixed capacitance per unit area, A is the detector area. In the second term, which describes the thermal noise from the FET channel resistance, Γ is the FET channel noise factor, g_m is the FET transconductance, and $I_3 = 0.0868$. The physical detection area of the PD considered here is 1.0 cm^2. The gain at the optical filter is 1.0, and the refractive index of the optical concentrator is 1.0. The O/E (optical to electrical) conversion efficiency of the typical PD is 0.54 A/W; we assume here a silicon PD whose peak sensitivity lies in the visible wavelength band. The spectral response at the PD is wavelength selective, whereas we can design the optical bandpass filter with multiple thin dielectric layers. Note also that white LEDs emit light over a wide wavelength. Consequently, we can use whatever wavelength yields the best response at the PD. We choose the following noise parameter values: $T_K = 298$ K, $G = 10$, $gm = 30$ mS, $\Gamma = 1.5$, $\eta = 112$ pF/cm^2, and $I_{bg} = 5100$ μA. The background current is a measured value using direct sun light [32].

III. Adaptive Equalization

A. Decision Feedback Equalization

The basic idea behind DFE is that once an information symbol has been detected and decided upon, the ISI that it induces on future symbols can be estimated and eliminated before detecting the subsequent symbols. The DFE can be realized in direct transversal form as shown in Fig. 4. It consists of a feedforward (FF) filter and a feedback (FB) filter. The FB filter is driven by decisions on the output of the detector, and its coefficients can be adjusted to cancel the ISI on the current symbol from past detected symbols. The equalizer has $N_{FF} + 1$ taps in the FF filter and N_{FB} taps in the FB filter, and its output can be expressed as [33]:

$$\hat{d}_k = \sum_{n=0}^{N_{FF}} c_n^* y_{k-n} + \sum_{i=1}^{N_{FB}} F_i^* d_{k-i}, \tag{15}$$

where c_n^* and y_n are tap gains and the inputs, respectively, to the FF filter, F_{ik}^* are tap gains for the FB filter, and $d_i (i < k)$ is the previous decision made on the detected signal. That is, d_k can be decided once $\hat{d}_k$ is obtained using Eq. (15). d_k along with previous decisions d_{k-1}, d_{k-2}, $\cdots$ are fed back into the equalizer, and $\hat{d}_{k+1}$ is obtained using Eq. (15).

B. Least Mean Square Algorithm

Since adaptive equalization can compensate an unknown and time-varying channel, it requires a specific algorithm to update the equalizer coefficients and track the channel variations. A wide range of algorithms exist that can adapt the filter coefficients, but we assume an LMS algorithm. The LMS equalizer is a common design that minimizes the mean square error (MSE) between the desired equalizer output and the actual equalizer output.

Here, we define the input signal to the equalizer as vector $\boldsymbol{y}_k$ where

$$\boldsymbol{y}_k = \begin{bmatrix} y_k & y_{k-1} & y_{k-2} & \cdots & y_{k-N} \end{bmatrix}^T, \tag{16}$$

and the weight vector can be written as

$$\boldsymbol{w}_k = \begin{bmatrix} w_{0k} & w_{1k} & w_{2k} & \cdots & w_{Nk} \end{bmatrix}^T. \tag{17}$$

It follows that when the desired equalizer output is known, the error signal e_k is given by

$$e_k = d_k - \hat{d}_k. \tag{18}$$

To compute the mean square error $|e_k|^2$ at time instant k, Eq. (18) is squared to obtain

$$\xi = E[e_k^* e_k]. \tag{19}$$

The LMS algorithm seeks to minimize the mean square error given in Eq. (19). The LMS algorithm is the simplest equalization algorithm and requires only 2N+1 operations per iteration. Letting variable n denote the sequence of iterations, LMS is computed iteratively by

$$\hat{d}_k(n) = \boldsymbol{w}_N^T(n) \boldsymbol{y}_N(n), \tag{20}$$

$$e_k(n) = d_k(n) - \hat{d}_k(n), \tag{21}$$

$$\boldsymbol{w}_N(n+1) = \boldsymbol{w}_N(n) + \mu e_k^*(n) \boldsymbol{y}_N(n), \tag{22}$$

where subscript N denotes the number of delay stages in the equalizer, μ is the step size that controls the convergence rate and stability of the algorithm, and vector $\boldsymbol{y}_N$ is the input signal to the equalizer. Therefore, the LMS equalizer maximizes the signal to distortion ratio at its output within the constraints of the equalizer tap length. The convergence rate of the LMS algorithm is slow due to fact that only one parameter, the step parameter μ, controls the adaptation rate.

C. Mean Square Error

In this section, we discuss the validity of the value of step parameter and the length of the training sequence for the BER performance at each position. Figure 5 shows the relation between MSE by the LMS algorithm and the length of training sequence at the receiver positions of (0.1, 2.1, 0.85) where the FF filter has 4 taps and the FB filter has 2 taps. At the position, the received optical power is -5.55 dBm/cm^2. The received optical power is determined by function of lighting equipment. The data drawn represents the average of 1000 trials. From the figure, we can see that the value of the step parameter has hardly influence on the MSE values at each data rate when

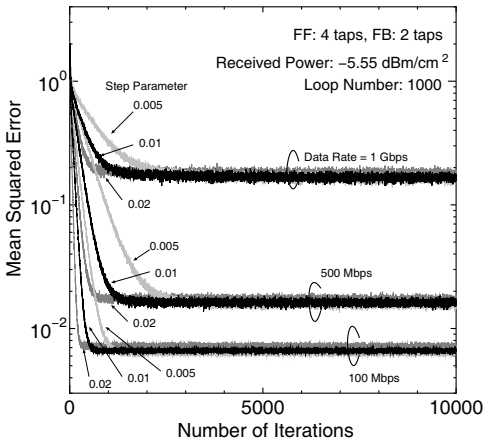

Fig. 5. Mean square error. Received optical power is -5.55 dBm/cm^2, loop number is 1000, FF: 4 taps, FB: 2 taps.

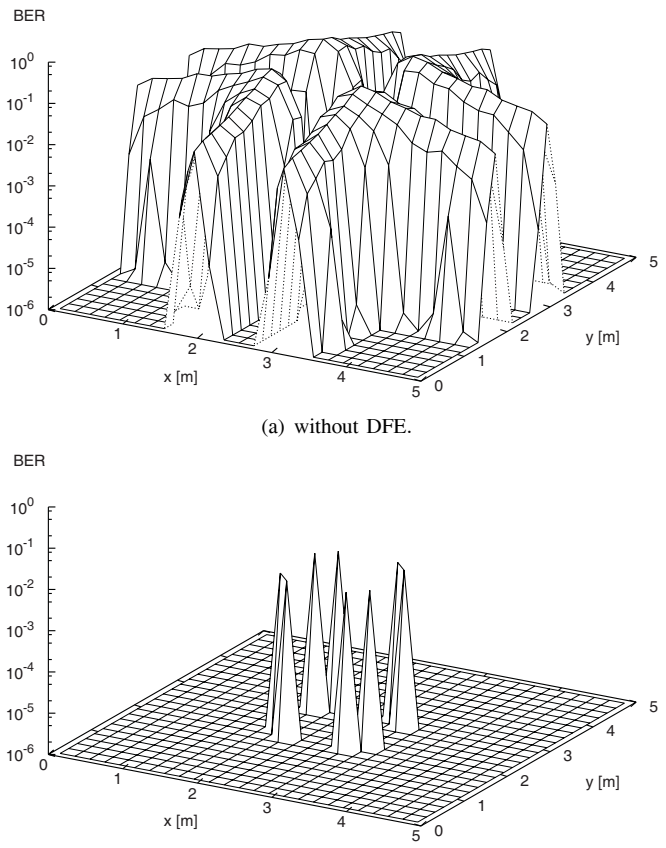

(a) without DFE.

(b) with DFE, FF tap is 4, FB tap is 2, step parameter is 0.01, training sequence is 10000 bits.

Fig. 6. BER distribution. Data rate is 500 Mbit/s.

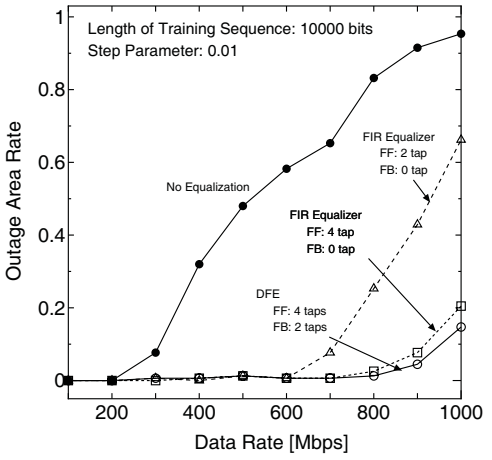

Fig. 7. Outage area rate versus data rate. Step parameter is 0.01, length of training sequence is 10000 bits.

the number of iterations is enough, but does determine the tracking ability of the LMS equalizer. The larger the step parameter is, the better the tracking ability of the equalizer becomes. However, large step parameters cause excess noise. We can also see that MSE yields high data rates since the received SNR depends on the data rate. From the result, for the following simulations, we set the number of iterations and the step parameter at 10000 and 0.01, respectively.

D. BER Performance

Figure 6 shows the distribution of BER performance versus receiver position on a 0.20 m grid. We can see that the low BER area is increased by DFE, which indicates high data rates. DFE effectively mitigates the influence of ISI. We can also see that the performance directly under the sources is degraded. Because, at these positions, the powers of first and second paths become approximately equal. Therefore, the consecutive paths, which have sub-equal power, cause error propagation.

Figure 7 shows the relation between data rate and outage area rate. We define the outage area rate as the ratio of the area where BER is larger than 10^{-6} to the total service area. We can see that increasing the data rate increases the outage area rate. A system with some taps FF filter and a 0 tap FB filters is an FIR equalizer (linear equalizer). We can see that the system with DFE effectively mitigates the ISI effects. When data rate is over 200 Mbit/s, the FIR equalizer and DFE are effective. The DFE is especially effective at data rates over 700 Mbit/s, compared with the FIR filter. And adaptive equalizer with few taps is improved the outage area rate performance, effectively.

E. Training Sequence Interval

We determine here the appropriate training sequence interval. Figure 8 show the BER performance achieved when the channel estimation weights estimated for position X are used at position Y. Here, in this simulation, we assume a static channel based on the calculated impulse response by ray-tracing. The horizontal axis is the distance between position X and Y. At 500 Mbit/s, there is no error by the use of inappropriate weights if the distance is below 0.283 m, so the weights should be updated every 0.283 m. Therefore, when a terminal moves at the speed of 3.6 km/h, the training sequence has to send at intervals of less 0.283 s. By setting the interval, the receiver can have seamless communication and high quality communication.

IV. Influence of Shadowing

In this section, we discuss the effect of shadowing on the adaptive equalization system assuming multiple sources with a

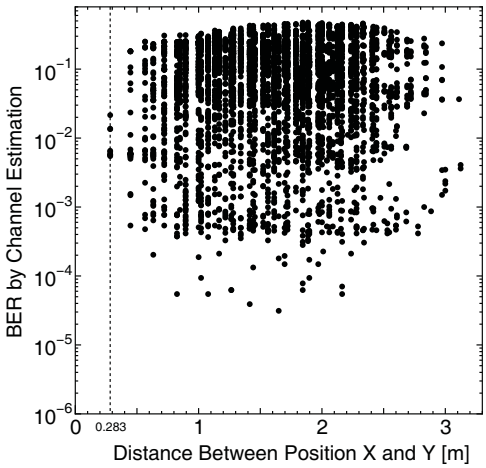

Fig. 8. Distance between position X and Y versus BER by channel estimation. Data rate is 500 Mbit/s. FF tap is 4, FB tap is 2, Step parameter is 0.01, length of training sequence is 10000 bits.

specific impulse response. Generally, lighting equipments are distributed within a room and the irradiance of light has a wide angle to function as lighting equipment, which helps minimize a shadowing effect. However, the signal from multiple lighting equipments causes the ISI. Therefore, there is a correlation between the influence of shadowing and the ISI. We consider downlink transmission based on time-division multiple access (TDMA) and perform theoretical analyses and computer simulations to evaluate the effects of shadowing caused by pedestrians. We show that the visible light communication system with adaptive equalization is robust against shadowing.

TABLE I
SIMULATION CONDITIONS FOR INFLUENCE OF SHADOWING.

Access Method	TDMA (considered only downlink)
Number of channels	10
Terminals	Uniform Distribution
Traffic Model	Poisson Arrival
Call Duration	Exponential Distribution
Mean Call Duration Time	20.0 [s]
Generation of Pedestrian	Exponential Distribution
Motion of Pedestrians	
Velocity	Uniform Distribution 0 to 4 [km/h] (constant)
Orientation	Uniform Distribution 0 to 2 π [rad.] (constant)
Walking Time	5.0 [sec.] (constant)

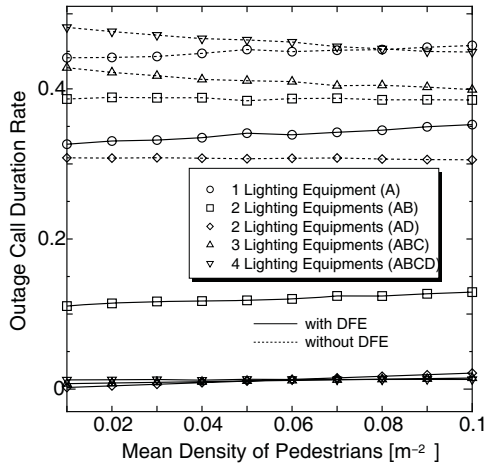

Fig. 9. Outage call duration rate versus mean density of pedestrians. Bit rate is 500 Mbit/s, the offered load is 4 erl.

A. Traffic Consideration

The call blocking performance of mobile wireless users in planar cellular arrays is generally determined using a Markov model [34]. In this paper, we assume that the network traffic follows the Markov model (M/M/S(0)).

Call arrivals are assumed to follow an independent Poisson process, one for each cell. We use λ, in units of calls per second per cell, for the call arrival rate. If τ is the mean call duration time (service time), then the call duration rate for one channel, measured when it is busy, is $\mu = \tau^{-1}$. The ratio $\chi = \lambda/\mu$ is the offered load, in Erlangs/cell.

The classical Erlang-B formula for the probability that a call in a cell is blocked in backbone network when there are c channels in the cell, is

$$P[\text{Blocking}] = \frac{\chi^c/c!}{\sum_{j=0}^{c} \chi^j/j!}. \tag{23}$$

B. Outage Call Duration Rate

The simulation parameters are shown in Table I. We consider downlink transmission based on TDMA. We assign a channel to different time slots in the same frequency band to each terminal. The terminal is generated in the room according to uniform distribution. And a call in the terminal is generated according to Poisson arrival. A position of the terminal is fixed during the connection. We assume that optical paths are hampered by pedestrian. We model the pedestrian as a column with diameter of 0.35 m and a height of 1.70 m [35]. The pedestrian is generated according to exponential distribution. And the training sequence sends at intervals of 0.2 seconds. Here, we define an outage call duration rate as the ratio of the total duration when the BER exceeds 10^{-6} to the total call duration [36].

Figure 9 show the relation between outage call duration rate and mean density of pedestrians in the model room. The mean density of pedestrians is included a concept of time. (For example, five pedestrians exist during 5 s per 100 s each. Here, the floor size is 5 $\times$ 5 m^2. The mean density of pedestrians is $(5[\text{pedestrian}] \times 5[\text{s}]/100[\text{s}])/(5[\text{m}] \times 5[\text{m}]) = 0.01[\text{m}^{-2}]$.) The offered load is set to 4 erl. The DFE system has a 4 tap FF filter and a 2 tap FB filter. For the system without DFE, we can see that increasing the number of sources does not improve the outage call duration rate. The best performance is achieved with 2 sources. And the performance with 1 source is overtaken with 4 sources. This is because, by increasing the mean density of pedestrians, the performance with 1 source is deteriorated, and the performance with 4 sources approaches that with 3 or 2 sources by blocking the optical paths cause ISI. In other words, the ISI is main cause of deterioration in this model. This confirms that there is a correlation between ISI and shadowing. We can see that the optimal number of source depends on the data rate, mean density of pedestrians, room model, and so on. In the system with DFE, the use of multiple

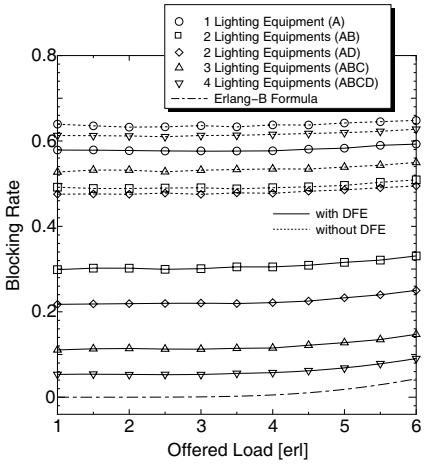

Fig. 10. Blocking rate versus offered load: bit rate is 500 Mbit/s, the mean density of pedestrian is 0.05 m^{-2}.

sources avoids outage call, by tracking the variable optical wireless channel and equalizing the received signal. Adaptive equalization is shown to greatly increases the probability of acceptable communication quality.

C. Blocking Rate

The blocking rate is defined as the ratio of the total duration when all 10 channels are occupied or calls are blocked or the BER exceeds 10^{-6} to the total of call duration [36].

Figure 10 shows the blocking rate versus the offered load. Here the performance with the Erlang-B formula corresponds to the performance achieved when no error occurs in the free-space optical environment. In a 500 Mbit/s system without DFE, we can see that using the optimal number of sources, 2(AD), can achieve the best blocking rate performance. This system approximates the performance indicated by the Erlang-B formula. Adding DFE improves the blocking rate performance. A 500 Mbit/s system with DFE and optimal number of sources, 4, can achieve the best blocking rate performance. This confirms that adaptive equalization system is very effective in countering the shadowing problem.

V. Conclusion

The visible-light free-space communication system described herein has much larger transmission power than infrared wireless communication systems since it also provides ambient lighting. It is seen as a very cost effective solution since lighting engineers will install many light sources on the ceiling to provide adequate a lighting throughout the room. From the viewpoint of communication engineers, transmission via LOS links without shadowing can be achieved because of the many lighting sources distributed across the ceiling. However the optical path difference between multiple sources causes ISI.

This paper proposed the use of an adaptive equalizer to overcome the ISI problem. The performance of an adaptive equalizer with LMS algorithm was evaluated. The results showed that for data rates of over 200 Mbit/s, FIR equalizer and DFE were very effective. When the data rate exceeded 700 Mbit/s, the DFE effectively mitigated the influence caused by ISI. We showed that the simple equalizer with few taps is very effective even if the data rate is 1 Gbit/s. And we elucidated the most effective training sequence interval for channel estimation. Moreover, the influence of shadowing with the multiple sources was discussed. An optimal number of the lighting equipment for communication on the model room was shown. And the optimal number of source depended on the data rate, mean density of pedestrians, room model, and so on. We showed that the system with adaptive equalization was robust against shadowing and could accommodate more calls.

The analyses and simulations presented here confirm that the proposed system is very promising for future high speed wireless access networks and it could be one of the choices for an indoor optical wireless data transmission system.

References

[1] S. Nakamura, "Present performance of InGaN based blue / green / yellow LEDs," in *Proc. SPIE Conference on Light-Emitting Diodes: Research, Manufacturing, and Applications*, vol. 3002, pp. 24–29, 1992.

[2] C. P. Kuo, R. M. Fletcher, T. D. Osentowski, M. C. Lardizabal, M. G. Craford, and V. M. Robbins, "High performance ALGaInP visible light-emitting diodes," *Applied Physics Lett.*, vol. 57, no. 27, pp. 2937–2939, 1990.

[3] Y. Tanaka, S. Haruyama, and M. Nakagawa, "Wireless optical transmissions with white colored LED for wireless home links," in *Proc. IEEE International Symposium on Personal, Indoor and Mobile Radio Communications*, vol. 2, pp. 1325–1329, 2000.

[4] T. Komine, Y. Tanaka, S. Haruyama, and M. Nakagawa, "Basic study on visible-light communication using light emitting diode illumination," in *Proc. International Symposium on Microwave and Optical Technology*, pp. 45–48, 2001.

[5] Y. Tanaka, T. Komine, S. Haruyama, and M. Nakagawa, "A basic study of optical OFDM system for indoor visible communication utilizing plural white LEDs as lighting," in *Proc. International Symposium on Microwave and Optical Technology*, pp. 303–306, 2001.

[6] T. Komine and M. Nakagawa, "Fundamental analysis for visible-light communication system using LED lights," *IEEE Trans. Consumer Electronics*, vol. 50, no. 1, pp. 100–107, 2004.

[7] T. Komine and M. Nakagawa, "Performance evaluation on visible-light wireless communication system using white LED lightings," in *Proc. Ninth IEEE Symposium on Computers and Communications*, vol. 1, pp. 258-263, 2004.

[8] K. Fan, T. Komine, Y. Tanaka, and M. Nakagawa, "The effect of reflection on indoor visible-light communication system utilizing white LEDs," in *Proc. 5th International Symposium on Wireless Personal Multimedia Communications*, pp. 611–615, 2002.

[9] Y. Tanaka, T. Komine, S. Haruyama, and M. Nakagawa, "Indoor visible light data transmission system utilizing white LED lights," *IEICE Trans. Commun.*, vol. E86–B, no. 8, pp. 2440–2454, 2003.

[10] T. Komine and M. Nakagawa, "Integrated system of white LED visible-light communication and power-line communication," *IEEE Trans. Consumer Electronics*, vol. 49, no. 1, pp. 71–79, 2003.

[11] T. Komine, S. Haruyama, and M. Nakagawa, "Performance evaluation of narrowband OFDM on integrated system of power-line communication and visible-light wireless communication," in *Proc. International Symposium on Wireless Pervasive Computing*, 2006.

[12] P. Amirshahi and M. Kavehrad, "Broadband access over medium and low voltage power-lines and use of white light emitting diodes for indoor communications," in *Proc. 3rd IEEE Consumer Communications and Networking Conference*, vol. 2, pp. 897–901, 2006.

[13] M. D. Audeh, J. M. Kahn, and J. R. Barry, "Decision-feedback equalization of pulse-position modulation on measured nondirected indoor infrared channels," *IEEE Trans. Commun.*, vol. 47, no. 4, pp. 500–503, 1999.

[14] D. C. M. Lee and J. M. Kahn, "Coding and equalization for PPM on wireless infrared channels," *IEEE Trans. Commun.*, vol. 47, no. 2, pp. 255–260, 1999.

[15] J. R. Barry, J. M. Kahn, W. J. Krause, E. A. Lee, and D. G. Messerschmitt, "Simulation of multipath impulse response for indoor wireless optical channels," *IEEE J. Select. Areas Commun.*, vol. 11, no. 3, pp. 367–379, 1993.
[16] K. Takaoka and G. Hatakoshi, "InGaAlP-based red VCSEL & RCLED," IEICE Technical Report, vol. LQE2000-128, pp. 51–56, 2001.
[17] D. C. O'Brien, *et al.*, "High speed integrated optical wireless transceivers for in-building optical LANs," in *Proc. SPIE Conference on Optical Wireless Communication III*, vol. 4214, Boston, USA, pp. 104–114, 2001.
[18] D. M. Holburn, R. J. Mears, and R. J. Samsudin, "A CMOS 155Mb/s optical wireless transmitter for indoor networks," in *Proc. SPIE Conference on Optical Wireless Communication III*, vol. 4213, Boston, USA, pp. 124–132, 2001.
[19] A. Ishizuka, K. Nakajima, and H. Koyano, "Simple packaging technologics for optical transceiver module adaptable to large core-diameter fiber link," *IEICE Trans. Electron.*, vol. J84-C, no. 9, pp.822-830, 2001.
[20] A. S. Glassner, *An Introduction to Ray Tracing*. San Diego, CA: Academic Press, 1989.
[21] A. Satoh and E. Ogawa, "Fundamental characteristics of in-house infrared propagation and environmental noise," in *Proc. IEEE Antennas and Propagation Society International Symposium*, pp. 205–208, 1986.
[22] F. R. Gfeller and U. Bapst, "Wireless in-house data communication via diffuse infrared radiation," *Proc. IEEE*, vol. 67, no. 11, pp. 1474–1486, 1979.
[23] J. M. Kahn, W. J. Krause, and J. B. Carruthers, "Experimental characterization of non-directed indoor infrared channels," *IEEE Trans. Commun.*, vol. 43, pp. 1613–1623, 1995.
[24] D. Hash, J. Hillery, and J. White, "IR RoomNet: model and measurement," IBM Communication ITL Conference, 1986.
[25] J. R. Barry, Wireless Infrared Communications. Boston, MA: Kluwer Academic Press, 1994.
[26] R. S. Berns, *Billmeyer and Saltzman's Principles of Color Technology*. John Wiley & Sons Inc., 2000.
[27] J. M. Kahn and J. R. Barry, "Wireless infrared communications," *Proc. IEEE*, vol. 85, no. 2, pp. 265–298, 1997.
[28] J. D. Parsons, The Mobile Radio Propagation Channel. New York: Halsted Press, 1992.
[29] D. Molkdar, "Review on radio propagation into and within buildings," *IEE Proc. H, Microwaves, Antennas and Propagation*, vol. 138, no. 1, pp. 61–73, 1991.
[30] R. M. Gagliardi and S. Karp, *Optical Communications*. McGraw-Hill, 1983.
[31] P. Djahani and J. M. Kahn, "Analysis of infrared wireless links employing multibeam transmitters and imaging diversity receivers," *IEEE Trans. Commun.*, vol. 48, no. 12, pp. 2077–2088, 2000.
[32] A. J. C. Moreira, R. T. Valadas, and A. M. O. Duarte, "Optical interference produced by artificial light," *Wireless Networks*, vol. 3, no. 2, pp. 131–140, 1997.
[33] T. S. Rappaport, *Wireless Communications: Principles and Practice*, 2nd ed. Prentice Hall PTR, 2002.
[34] G. J. Foschini, B. Gopinath, amd Z. Miljanic, "Channel cost of mobility," *IEEE Trans. Veh. Technol.*, vol. 42, no. 4, pp. 414–424, 1993.
[35] T. Komine, S. Haruyama, and M. Nakagawa, "A study of shadowing on indoor visible-light wireless communication utilizing plural white LED lightings," *Wireless Personal Commun.*, vol. 34, no. 1–2, pp. 211–225, 2005.
[36] A. Sato, T. Otsuki, and I. Sasase, "A study of shadowing on non-directed LOS indoor wireless system with site diversity," *IEICE Trans. Commun.*, vol. J83–B, no. 12, pp. 1692–1701, 2000.

Toshihiko Komine was born in Shizuoka, Japan, on November 17, 1978. He received the B.E., M.E., and Ph.D. degrees in Information and Computer Science from Keio University, Yokohama, Japan, in 2001, 2003, and 2006, respectively. He joined KDDI Corporation in 2006, and has been engaged in research and development of digital radio transmission techniques for mobile communications at KDDI R&D Laboratories, Inc..

Jun Hwan Lee was born in Seoul, Korea on January 24, 1972. He received his B.E from Kwangwoon University, Seoul, Korea in 1997, and M.E from KJIST (Kwangju Institute of Science and Technology), Kwangju, Korea in 2000. In March 2000 he joined in ETRI (Electronics and Telecommunications Research Institute) until October 2003. At the time he was a staff of smart antenna team. Currently he is a Ph.D. student in the Department of Information and Computer Science, Keio University. His research interests include an equalizer design in wideband spread spectrum technique, and ISI and ICI canceller in multicarrier communication.

Shinichiro Haruyama is a visiting professor at Department of Information and Computer Science, Faculty of Science and Technology, Keio University, Yokohama, Japan. He received an M.S. in engineering science from University of California at Berkeley in 1983 and a Ph.D. in computer science from the University of Texas at Austin in 1990. He worked for Bell Laboratories of AT&T and Lucent Technologies, U.S.A from 1991 to 1996, and for Sony Computer Science Laboratories, Inc. from 1998 to 2002. His research interests include reconfigurable system, system design automation, wireless communication, and visible light communication.

Masao Nakagawa was born in Tokyo Japan in 1946. He received the B.E., M.E., and Ph.D. degrees in electrical engineering from Keio University, Yokohama, Japan, in 1969, 1971 and 1974 respectively. Since 1973, he has been with the Department of Electrical Engineering, Keio University, where he is now Professor.

His research interests are in CDMA, Consumer Communications, Mobile Communications, ITS (Intelligent Transport Systems), Wireless Home Networks, and Visible Optical Communication. He is a co-author of TDD-CDMA for Wireless Communications published by Artech House Publishers in 2003 in which the original ideas of TDD-CDMA followed by TD-CDMA in the world standard@IMT-2000 and Pre-Rake were given by him. He published more than 120 journal papers and more than 150 international conference papers.

He was the executive committee chairman of International Symposium on Spread Spectrum Techniques and Applications in 1992, the technical program committee chairman of ISITA (International Symposium on Information Theory and its Applications) in 1994, and the general chairman of WPMC (Wireless Personal Mobile Communications) in 2003. He is an editor of WIRELESS PERSONAL COMMUNICATIONS (European journal) and was a guest editor of the special issues on "CDMA Networks I, II, III and IV" published in IEEE JSAC in 1994 (I and II) and 1996 (III and IV). He chairs the Visible Light Communications Consortium. He is an NHK (Nippon Broadcasting Cooperation) Technical Council member.

He received IEEE Consumer Electronics Society Paper Award in 1989, 1999-Fall Best Paper Award in IEEE Vehicular Technology Conference in Amsterdam, IEICE Achievement Award in 2000, IEICE Fellow Award in 2001, Information Month Award of Ministry of Internal Affairs and Communications in 2001, Ericsson Telecommunications Award in 2004, YRP Award in 2005, and IEEE Fellow Award for contributions to CDMA and mobile communications in 2006.